Observations of the Gamow-Teller resonance in the rare-earth nuclei above ^{146}Gd populated in β decay

E. Nácher,[1,*] B. Rubio,[1,†] A. Algora,[1,‡] D. Cano-Ott,[1,§] J. L. Taín,[1] A. Gadea,[1] J. Agramunt,[1] M. Gierlik,[2] M. Karny,[2] Z. Janas,[2] E. Roeckl,[3] A. Blazhev,[3,‖] R. Collatz,[3] J. Döring,[3,¶] M. Hellström,[3] Z. Hu,[3] R. Kirchner,[3,#] I. Mukha,[3] C. Plettner,[3] M. Shibata,[3] K. Rykaczewski,[4] L. Batist,[5] F. Moroz,[5] V. Wittmann,[5,**] and J. J. Valiente-Dobón[6,††]

[1]*IFIC, CSIC-Universidad Valencia, Apartado Postal E-22085, 46071 Valencia, Spain*

[2]*Faculty of Physics, University of Warsaw, PL-02-093 Warsaw, Poland*

[3]*Gesellschaft für Schwerionenforschung, D-64291 Darmstadt, Germany*

[4]*Physics Division, Oak Ridge National Laboratory, Oak Ridge, Tennessee 37831-6371, USA*

[5]*St. Petersburg Nuclear Physics Institute, 188-350 Gatchina, Russia*

[6]*Department of Physics, University of Surrey, Guildford GU2 5XH, United Kingdom*

(Received 26 October 2015; published 13 January 2016)

The rare-earth region of the nuclear table around the quasi-doubly magic nucleus ^{146}Gd is one of the very few places in which the Gamow-Teller (GT) resonance can be populated in β decay. The appropriate technique to study such a phenomenon is total absorption spectroscopy, thanks to which one can measure the B(GT) distribution in β-decay experiments even when it is very fragmented and lies at high excitation energy in the daughter nucleus. Results on the GT resonance measured in the β decay of the odd-Z, $N = 83$ nuclei ^{148}Tb, ^{150}Ho, and ^{152}Tm are presented in this work and compared with shell-model calculations. The tail of the resonance is clearly observed up to the limit imposed by the Q value. This observation is important in the context of the understanding of the "quenching" of the GT strength.

DOI: 10.1103/PhysRevC.93.014308

I. INTRODUCTION

β-decay studies are among the most powerful tools one can use to understand the nuclear structure of atomic nuclei. The process itself is well understood and has been known for many years. The operators responsible for the transition between the parent state and the states populated in the daughter nucleus—the $\sigma\tau$ in the case of Gamow-Teller or the τ operator in the case of Fermi—are simple and selective, and, therefore, when the transition is allowed, the study of the β decay is an attractive tool to check nuclear models. In the first case, Gamow-Teller (GT), the transition between the parent and the final state in the daughter nucleus can change one unit in spin as well as in isospin; in the second case, Fermi, only the third component of the isospin changes. If we look at this process from the shell-model single-particle point of view, we can imagine β^+ (β^-) as the process where a *proton* (*neutron*) is transformed into a *neutron* (*proton*), and the transition can occur between identical orbits (Fermi and GT) or between spin-orbit partners (GT).

If we restrict ourselves to β^+ decay, the subject of this article, and for nuclei with $Z < N$, the Fermi transitions are forbidden, and the GT transitions are, in general, severely hindered [1]. The reason for the hindrance is that in transforming the available protons into neutrons the corresponding allowed orbitals on the neutron side are often occupied. There are, however, some exceptions, for instance, in $N \approx Z$ nuclei around mass 70–80 [2–4], where protons and neutrons fill orbitals with the same quantum numbers. The other possibility is when protons fill a certain orbital $J_>$ and its spin-orbit partner $J_<$ is still empty on the neutron side. Two such examples are the nuclei around ^{100}Sn [5–8], where protons from the intruder orbital $g_{9/2}$ can decay to the empty or partially occupied $g_{7/2}$ orbital on the neutron side, and the rare-earth nuclei above ^{146}Gd [9], in which the intruder $h_{11/2}$ orbital is being filled with protons that can decay to the empty $h_{9/2}$ neutron orbital. The latter case is the subject of the present work.

^{146}Gd has a very special feature only shared by the doubly magic ^{208}Pb; it is an even-even nucleus but its first excited state has spin-parity $J^\pi = 3^-$ instead of 2^+ like most of the other even-even nuclei [10,11]. However, the transition probability [B(E3)] from this state to the ground state is very large, a factor of ≈37 compared with the single-particle estimate [11]. The same effect occurs in ^{208}Pb, and it is a clear indication of the highly collective character of the 3^- state. These similarities between the two nuclei made people think of ^{146}Gd as a new doubly magic nucleus. Although this is clearly not the case, it is possible to consider ^{146}Gd as a doubly-closed-shell nucleus in many respects. For instance, the existence of a double octupole state with $J^\pi = 6^+$ and its characteristic deexcitation cascade of two $E3$ electromagnetic transitions ($6^+ \rightarrow 3^- \rightarrow 0^+$) has long been sought in ^{208}Pb as well as in ^{146}Gd but it has only recently been observed in the latter [12].

*Present address: Instituto de Estructura de la Materia, CSIC, Serrano 113-bis, E-28006 Madrid, Spain.

†berta.rubio@ific.uv.es

‡On leave from Institute of Nuclear Research, Debrecen, Hungary.

§Present address: Centro de Investigaciones Energéticas Medioambientales y Tecnológicas, E-28040 Madrid, Spain.

‖Present address: Institut für Kernphysik, Universität zu Köln, D-50937 Cologne, Germany.

¶Present address: Bundesamt für Strahlenschutz, D-10318 Berlin, Germany.

#Deceased.

**Deceased.

††Present address: INFN-Laboratorio Nazionale di Legnaro, 35020 Legnaro (PD), Italy.

Following the shell-model approach, there are five orbitals between the magic numbers 50 and 82: $1g_{7/2}$, $2d_{5/2}$, $3s_{1/2}$, $1h_{11/2}$, and $2d_{3/2}$. ^{146}Gd has 64 protons and 82 neutrons. Obviously, it is magic in neutrons, but the filled proton orbitals $1g_{7/2}$ and $2d_{5/2}$ are well separated from $3s_{1/2}$, $1h_{11/2}$, and $2d_{3/2}$. Subtracting the separation energy for protons in ^{146}Gd and ^{147}Tb and correcting for pairing correlations, an energy gap of ≈2.4 MeV between $2d_{5/2}$ and the group of three free orbitals $3s_{1/2}$, $1h_{11/2}$, and $2d_{3/2}$ (which lie within ≈260 keV of each other) [13] is obtained. In this article we deal with nuclei with $Z > 64$ and $N > 82$. These nuclei will be interpreted in terms of a few valence particles outside the ^{146}Gd core.

If we treat nuclei in this region as a ^{146}Gd core plus a number of extra active particles, then, as we add protons to the core (^{147}Tb, ^{148}Dy , . . .), we start filling the upper orbitals $3s_{1/2}$, $1h_{11/2}$, and $2d_{3/2}$. Among them, only $h_{11/2}$ presents the possibility of an allowed GT decay $\pi h_{11/2} \rightarrow \nu h_{9/2}$. In this work we study this allowed transition as we increase the number of protons filling the $h_{11/2}$ orbital. In principle, one might think that the best cases to study this decay are the $N = 82$ isotones. However, the odd-proton $N = 82$ nuclei have two low-lying states that β decay, one of them being the g.s. and the other an isomeric state. Any radioactive samples produced at mass separators will be a mixture of these two activities and consequently be difficult to disentangle in a β-decay experiment. Thus, if we study the $N = 82$ cases we are limited to the even-even cases and therefore only to the decay of protons pairs in the $h_{11/2}$ orbital. Alternatively, if we study the $N = 83$ cases there is no experimental problem because, even though the odd-Z, $N = 83$ isotopes also have two β-decaying states (for the sake of simplicity we refer to them as isomers, although one of them will be the g.s.)—one with spin-parity $J^\pi = 2^-$ and the other $J^\pi = 9^+$—they can be produced selectively by means of fusion-evaporation reactions. We see later that the most likely configuration of the low-spin isomer corresponds to an even number of protons in the $h_{11/2}$, whereas the high-spin isomer will have one more unpaired proton in this orbital. In other words, measuring the odd-Z, $N = 83$ isotopes above ^{146}Gd, namely ^{148}Tb, ^{150}Ho, and ^{152}Tm, we can cover the systematics of the $\pi h_{11/2} \rightarrow \nu h_{9/2}$ decay in the region as we fill the $h_{11/2}$ orbital with approximately 0 to 5 protons. In this work we describe the measurement and analysis of the odd-Z, $N = 83$ nuclei ^{148}Tb and ^{152}Tm. The other odd-Z, $N = 83$ nucleus which is part of the systematics is ^{150}Ho already analyzed by Cano *et al.* [14] and presented elsewhere [15].

In the three odd-Z, $N = 83$ cases the low-spin isomer (2^-) can be well described by the configuration $[\pi d_{3/2}\ \nu f_{7/2}]_{2^-}[\pi^{2n}]_{0^+}$, and the high-spin isomer by the configuration $[\pi h_{11/2}\ \nu f_{7/2}]_{9^+}[\pi^{2n}]_{0^+}$. In both cases, the second term represents n pairs of protons coupled to 0^+ which, owing to pairing correlations, partially occupy the three proton orbitals $d_{3/2}$, $s_{1/2}$, and $h_{11/2}$. Although this picture is only an approximation to reality, it cannot be too far wrong because in the framework of the proposed orbitals there is no other combination of one proton and one neutron producing either 2^- or 9^+ low-lying states. The β decay of the low-spin isomer can only happen by breaking a proton pair $[h^2_{11/2}]_{0^+}$, whereas the high-spin isomeric decay (9^+) will have two possible decays, one corresponding to the breakup of the proton pair $[h^2_{11/2}]_{0^+}$, just as in the 2^- decay, and the other to the decay of the unpaired proton in the $h_{11/2}$ orbital necessary to make the 9^+. This extreme single-particle point of view is described in Fig. 1. The proton pair of the figure represents in reality an undefined number of proton pairs which will be close to zero in the case of ^{148}Tb, one for ^{150}Ho, and two in the case of ^{152}Tm. Owing to pairing correlations there is always the possibility of promotion of pairs across the gap at $Z = 64$. This is the only way to have nonzero occupation in the $h_{11/2}$ orbital in the case of the ^{148}Tb 2^- state and thus observe an allowed decay.

Assuming the extreme single-particle approach explained above, we can predict what we should observe in the decay of these isomers. In principle, the decay of the odd proton in the high-spin case will populate only one very well defined state in the daughter nucleus with spin parity 8^+. This state, in the even-even daughter nucleus, is of two-particle (2p) character. However, β decay breaking the proton pair in both the low- and

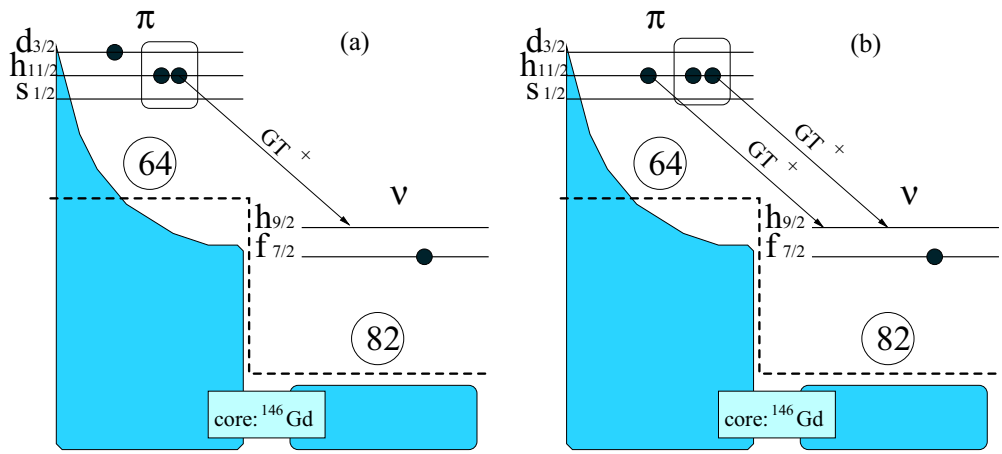

FIG. 1. Extreme single-particle representation of the configuration of the two isomers in the odd-Z, $N = 83$ isotopes above ^{146}Gd and their allowed GT decay. Panel (a) represents the low-spin isomer and panel (b) the high-spin one. The shaded region represents the occupation of proton pairs that may cross the gap at $Z = 64$ and the neutron occupation.

high-spin cases can populate states with spins 1^-, 2^-, 3^- in the case of the low-spin isomer decay and 8^+, 9^+, 10^+, in the case of the high-spin isomer. They have four-particle (4p) character and lie at higher excitation energy. One can make a rough estimate of the excitation energy of these states. The 2p states will lie at twice the pairing energy for protons (the energy necessary to break a proton pair) plus the single-particle energies of the two protons. The 4p state energy will require two times the proton pairing energy, plus two times the neutron pairing energy plus the four single-particle energies. In general terms, we can expect the 2p state at 2 to 2.5 MeV excitation energy and the $4p$ states at 4 to 5 MeV.

In this work we study the decay of 2^- and 9^+ isomers of ^{148}Tb and ^{152}Tm, and, for completeness, we include the results from Ref. [14,15] for the decay of the two isomers in ^{150}Ho in our discussion. We describe in detail only the experiment and the analysis performed in the ^{152}Tm 2^- case. In the other cases the same accelerator facility, mass separator, and total absorption spectroscopy (TAS) detector have been used, and the analysis techniques are very similar. Therefore, in the following we present a description of the experimental facility at GSI (not anymore existing), where the experiments were performed, a detailed description of the experiment and analysis of the decay of ^{152}Tm, and the results for all the different decays studied here. Finally, we perform shell-model calculations to compare with our results for the systematics of the GT transition in the region.

II. THE EXPERIMENTAL TECHNIQUE

To determine the B(GT), it is necessary to know the half-life of the parent nucleus, its Q_{EC} value, and the β population to each excited state in the daughter nucleus, from now on referred to as the β intensity distribution. The correct determination of the latter, which is normally extracted from the β-delayed γ's, is often the most difficult part. Traditionally, it is determined from the difference between γ intensity feeding and deexciting each level in the decay scheme constructed using Ge detectors. Unfortunately, in medium to heavy nuclei this kind of measurement is often affected by the so-called Pandemonium effect [16]. Owing to the low efficiency of the Ge detectors, to the fragmentation of the β intensity in regions of high-level density and to the fragmentation of the γ intensity deexciting each level, a big part of the β intensity at high excitation energy may be unobserved and erroneously misplaced at low excitation energy.

The alternative experimental method used in this work, the TAS technique [17], has been shown to overcome these difficulties (see Ref. [18] and references therein). The main idea is to build a detector with very high intrinsic efficiency for γ rays and very good geometrical coverage, as close as possible to 4π around the radioactive sample. In this way one can detect the complete γ cascades produced after the β decay rather than individual γrays, and in this way determine the β intensity at the right excitation energy.

The characteristics mentioned above were fulfilled by the TAS coupled to the On-line Mass separator at GSI [19,20]. In Fig. 2 this detector and the tape system which transports the radioactive source from the collection point to the measuring

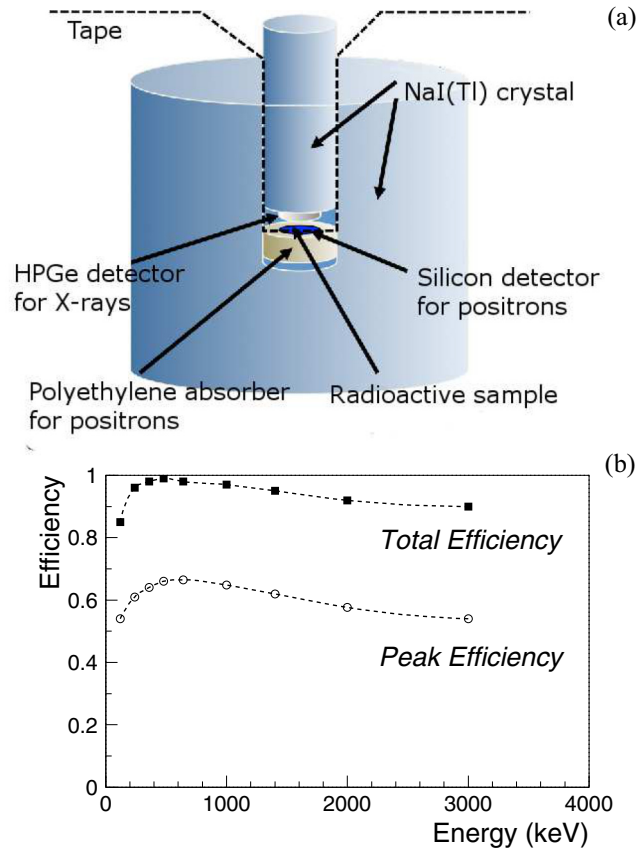

FIG. 2. Total absorption spectrometer at the GSI on-line mass separator (a). Simulated total and photo-peak efficiency for individual γ rays at several energies (b). Note that in the β^+/EC decays of interest the γ multiplicity is, in general, larger than 1, which makes the total efficiency close to 1 for most of the cases.

position inside the detector are shown schematically. As we see, the main NaI crystal is a cylinder ($\varnothing = h = 35.6$ cm) with a hole in the direction of the symmetry axis, forming a well. The upper part of the well is closed by a plug detector. The end of the plug holds the ancillary detectors: one germanium planar detector ($\varnothing$16 mm $\times$ 10 mm) to measure the x rays and tag electron capture processes and two silicon detectors to measure the positrons and tag β^+-decay processes. The top silicon detector ($\varnothing$17.4 mm $\times$ 0.5 mm) sees the source from above, and the bottom silicon detector, below the source, was, in reality, a telescope ($\varnothing$17.4 mm $\times$ 35 μm and $\varnothing$27.4 mm $\times$ 0.55 mm) to measure not only positrons but also protons or α particles. Below the bottom silicon detector there is a piece of beryllium which acts as absorber for the positrons. This is used to minimize the penetration of the charged particles into the crystal. One should note that the silicon-absorber mounting can be changed and has been altered for the different experiments. In particular, when measuring the ^{150}Ho and ^{148}Tb β decays the bottom silicon detector was a single detector and the absorber was polyethylene instead of beryllium.

One of the experimental challenges in the study of the odd-Z, $N = 83$ isotopes investigated in this work was the production of one specific isomer and not the other. For this

purpose we made use of the fact that the 2^- isomer is the only one populated in the β decay of the even-Z, $N = 82$ parent nucleus. This decay proceeds mainly through a fast GT transition to a 1^+ state which, in turn, decays by an $E1$ transition to the 2^- state of interest [9,21]. In particular, we produced ^{152}Tm 2^- through the β decay of the even $Z, N = 82$ ^{152}Yb. The β decay of this nucleus proceeds with 87.2% intensity to a 1^+ state at 482 keV energy in ^{152}Tm that decays to the 2^- isomer [21] (the remaining 12.8%, populating other 1^+ states, will also deexcite to the 2^- state and will never populate the 9^+ isomer). Summarising, we have produced the ^{152}Tm 2^- isomer activity very cleanly by producing and separating ^{152}Yb. The fusion-evaporation reaction chosen was ^{96}Ru(^{58}Ni,$2p$)^{152}Yb. The energy of the ^{58}Ni beam was degraded using a Ta foil and the ^{92}Mo target backing (facing the beam) from 5.30 down to 4.53 MeV/u when entering the target. The target was made of ^{96}Ru (96.53%) and had a thickness of 2.0 mg/cm^2.

After the reaction, the products entered a FEBIAD (Forced Electron Beam Induced Arc Discharge)-type ion source [22]. There an electron beam ionized the products to a 1^+ charge state and the ions were extracted with a 55-kV electrostatic potential. The separator magnet was set to select mass 152. The radioactive beam of this mass was then deflected vertically, implanted on the tape and moved periodically to the measuring position inside the TAS (see Fig. 2). As the measuring point was in air and the beam came through a pipe with a quite high vacuum, a differential pumping system was used to move the source implanted on the tape from vacuum to 1 atm. Once every eight cycles the separated radioactive beam was deflected to another tape transport system coupled to a measuring station equipped with a Ge detector at the ground level. During this cycle the TAS was measuring background and the Ge detector was used to monitor the production of the isotope of interest. The collection-measurement cycle was chosen to be symmetric and of 16 s. The trigger of the data-acquisition system required a signal in the TAS detector (main NaI crystal or plug detector). The direct spectra registered during the run under the conditions explained above are shown in Fig. 3, in which panel (a) shows the TAS spectrum, whereas the Ge-planar spectrum is plotted in panel (b). It shows the characteristic x rays associated with the different activities present in the source. As can be seen, the spectrum is dominated by the x rays of Er originating from the ^{152}Tm EC decay, although the Yb and Er activities are also present. In the following we describe how we have analyzed the EC component of the ^{152}Tm decay. To this aim we have selected events in the TAS in coincidence with the Er x rays, using the gates shown in the bottom panel of Fig. 3. The analysis of the EC component of the decay has two advantages over the analysis of the β^+ component. First, and most importantly, the resulting TAS spectrum is very clean, and second, the EC component extends up to 1022 keV more in excitation energy than the β^+ component. Once the EC-decay intensity distribution is obtained, the total EC + β^+ distribution can be calculated using the tabulated EC/β^+ values [23] and the $Q_{\rm EC}$. As mentioned above, the direct TAS spectrum is shown in the top part of the figure. Even though this spectrum contains the EC and β^+ component of all the activities present in the source plus the environmental background, one can already

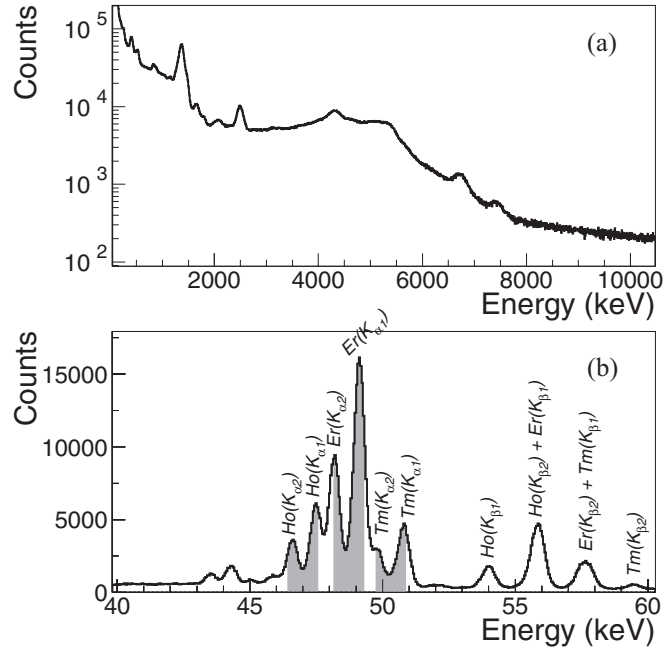

FIG. 3. Direct spectra obtained in the ^{152}Tm 2^- decay measurement in the TAS (a) and in the x-ray detector (b). The shaded regions represent the gates used in the analysis (see text).

discern a broad resonancelike structure between 4000 and 6000 keV. The TAS spectrum after setting up the gates on the Er(K$_{\alpha 1}$) and Er(K$_{\alpha 2}$) x-ray peaks is shown in Fig. 4(a) in black.

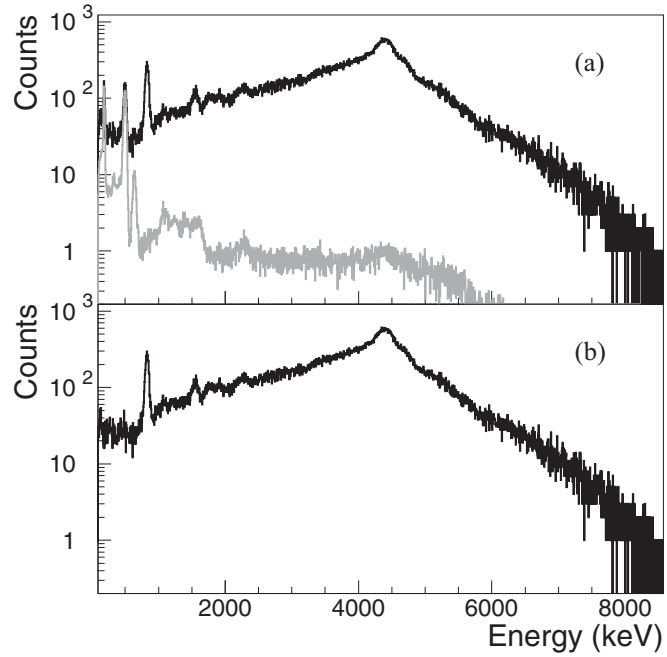

FIG. 4. (a) The TAS spectrum obtained by setting gates on the characteristic Er x rays in the ^{152}Tm$_{2^-}$ measurement is shown in black, and the spectrum of the relevant contaminants is shown in gray; see text. (b) The resulting TAS spectrum of ^{152}Tm$_{2^-}$ after the subtraction of the contaminants.

Unfortunately, even with these very conservative (narrow) gates, some counts coming from the tails of the neighboring x-ray peaks, namely Ho($K_{\alpha 1}$) and Tm($K_{\alpha 2}$), are present in the spectrum. A spectrum gated on these two contaminants is shown in Fig. 4(a) in light gray. It was constructed using the Tm and Ho x-ray gates, normalized with factors estimated using the peaks at 482 keV (^{152}Yb decay) and 180 keV (^{152}Er decay) visible in the TAS spectrum. In Fig. 4(b) the resulting spectrum obtained after the subtraction of the spectrum of contaminants is plotted.

III. ANALYSIS OF THE DATA: THE EXPECTATION-MAXIMIZATION ALGORITHM

In ideal conditions, if the TAS had 100% peak efficiency for γrays over the whole energy range, the experimental spectrum measured in the TAS would provide the β intensity distribution folded with the energy resolution of the crystal and the response of the detector to the positron when applicable. In reality, it is impossible to construct such an ideal TAS owing to the limited intrinsic efficiency of available scintillator crystals and the limited solid angle one can cover. Moreover, dead material inside the spectrometer such as the canning of the NaI or the ancillary detectors further reduces the γ efficiency. Another important point is the absorption in the TAS of other kinds of radiation produced in the decay such as β particles or the bremsstrahlung produced by them. In practice, this means that what we obtained is related to the β intensity through the response function of the spectrometer. A nontrivial deconvolution analysis and a very well determined response function are essential if we wish to extract an accurate β intensity distribution. The method used to construct the response function is explained in Ref. [24], and the method of carrying on the deconvolution process is based on the expectation maximization (EM) algorithm [25] adapted to the specific case of TAS data in Refs. [26,27]. As explained there the response function must be determined for each experiment because it depends, first, on the specific set up and, second, on each particular decay. In the following we explain how this was done in the present case.

The first thing we need at this stage is to calculate the response of the detector to γ and β radiation as a function of energy and validate it with a well-known source. We used the GEANT4 code [28] for the Monte Carlo simulations and a ^{24}Na source for the validation. In Fig. 5 we show the simulation of the ^{24}Na source compared with the measured one. The gray shaded area shows the measured TAS spectrum from the β decay of ^{24}Na. It is overlaid with the simulated spectrum shown as the dashed black line. The agreement is remarkably good.

The following step is to construct the response function of the detector for the specific case of interest. For this purpose we need to know the decay scheme to some extent. More specifically we need to know the deexcitation pattern of the levels populated in the decay. In the case of ^{152}Tm we have used the information provided in Ref. [29] supplemented with a preliminary evaluation of data for the same decay taken with the six Ge-cluster detectors at GSI. This provided reliable data up to 2129.0 keV and from that point on we have used the

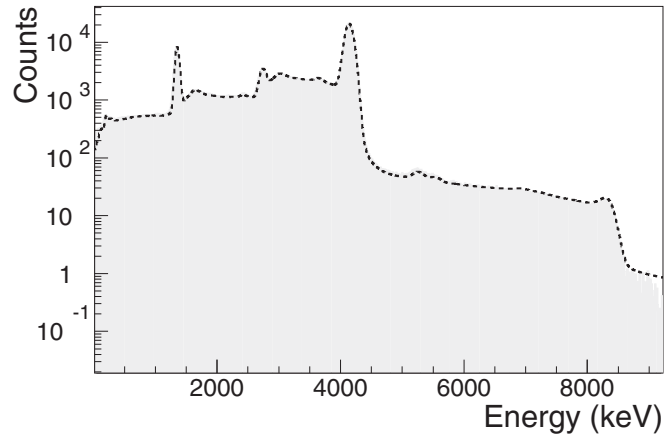

FIG. 5. Simulation of the β decay of ^{24}Na (dashed black line) overlaid to the measured ^{24}Na source (gray shade). The counts beyond the Q_β value correspond to pileup events.

statistical model. The parameters for the backshifted Fermi gas model were $a = 14.99$ MeV^{-1} and $\Delta = 0.69$ MeV [30,31]. These parameters were extracted from experimental data but are also consistent with the parametrization of Ref. [32]. For the branching ratios the parametrizations of Refs. [33,32], and [34,35] were used for the $E1$, $M1$, and $E2$ transitions respectively. The whole procedure is similar to that described in detail in Ref. [26].

After constructing the response function we have used the EM algorithm to unfold the experimental data. The resulting intensity distribution is shown in Fig. 6(b). With these results and the calculated response matrix we expect to reproduce the experimental spectrum as a quality check on our results.

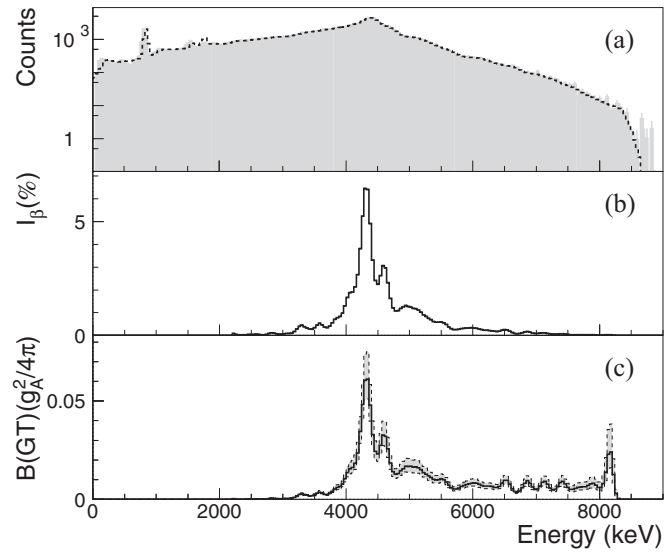

FIG. 6. (a) Experimental spectrum measured for the ^{152}Tm 2^- EC decay (gray shade). Overlaid, there is the recalculated spectrum using the results after the analysis and the response function (dashed line). (b) Resulting intensity distribution $I_\beta(E)$ after unfolding the data. (c) ^{152}Tm 2^- β-decay B(GT) distribution. The gray shading represents the uncertainty.

This is shown in the top panel of the same figure (a), where the gray shading shows the experimental spectrum and the dashed line the recalculated one, constructed by folding the intensity distribution obtained (b) with the response matrix calculated previously. We can see that the recalculated spectrum reproduces the measured spectrum remarkably well. As anticipated earlier, a strong and very narrow resonance is evident in the intensity distribution at ≈4.3 MeV excitation energy in ^{152}Er.

Once we have extracted the β intensity distribution from the experimental data, we can calculate the β strength using the following expression:

$$S_\beta(E) = \frac{I_\beta(E)}{f(Q_\beta - E)\, T_{1/2}}. \quad (1)$$

Then from the β strength one can easily calculate the B(GT) with Eq. (2). The units of the β strength S_β and the B(GT) in these equations are, respectively, s^{-1} and $g_A^2/4\pi$,

$$B(\mathrm{GT})(E) = K\left(\frac{g_V}{g_A}\right)^2 S_\beta(E), \quad (2)$$

where $K = 6143.6(17)$ [36] and $g_A/g_V = -1.270(3)$ [37]. It should be noted here that, even though the β intensity distribution I_β is defined for every possible excitation energy in the daughter nucleus E, it has been rebinned in 40-keV intervals during the analysis procedure. The reason is that the response function of our detector has been calculated in bins of 40 keV and the resulting B(GT) is therefore in 40-keV energy bins as well.

As we can see in Eq. (1), besides the β-intensity distribution $I_\beta(E)$ extracted from the present experiments, one needs the β-decay half-life and the Q_{EC} value. We have used the half-life $T_{1/2}(^{152}\mathrm{Tm}_{2^-}) = 8.0(10)$ s measured in Ref. [38] and confirmed in Ref. [29]. For the Q_{EC} value we have used Q_{EC} $(^{152}\mathrm{Tm}_{2^-}) = 8720(70)$ keV, taken from the Atomic Mass Evaluation of 2012 (AME2012) [39]. Moreover, we have extracted an independent value based on the end-point energy of the EC spectrum in the TAS, Q_{EC} $(^{152}\mathrm{Tm}_{2^-}) =$ 8820(240) keV, which is compatible with the one given in the AME2012 compilation but with a larger uncertainty. For the high-spin isomer of ^{152}Tm the situation is different: There is no experimental measurement of its Q_{EC} value. Its mass excess is given in the NUBASE2012 compilation [40] based on systematics. This is the reason why, in this case, we have used the value we obtained using the end point of the EC spectrum in the TAS detector as in Ref. [41] (see Fig. 7):

$$Q_{\mathrm{EC}}\,(^{152}\mathrm{Tm}_{9^+}) = 8680(240)\,\mathrm{keV},$$

which agrees with the NUBASE2012 value of 8834(100) keV estimated from systematics [40].

Using the above-mentioned values and the statistical rate Fermi integral tabulated in Ref. [23], we obtained the B(GT) distribution shown in Fig. 6(c). We can observe the strong resonance peaked at ≈4.3 MeV excitation energy in ^{152}Er, already visible in the $I_\beta(E)$, and now a tail which extends up to the Q_{EC} value. One can observe oscillations in the strength distributions above 6.5 MeV. These are likely to be artifacts produced by the deconvolution procedure related to the low statistics at the end of the spectrum. The oscillations in the β intensity are enhanced by the Fermi function (see discussion in Ref. [27]). In particular, the peak at the end of the distribution was removed from the evaluation of the B(GT) because it is regarded unphysical. The gray shading in the figure is the uncertainty and is mainly attributable to the uncertainties in the Q_{EC} (largest contribution) and the half-life values. These uncertainties also propagate to the sum of the B(GT), which gives a value of $\sum^{8.0\,\mathrm{MeV}} B(\mathrm{GT})_{2^-} = 1.3(2)\frac{g_A^2}{4\pi}$.

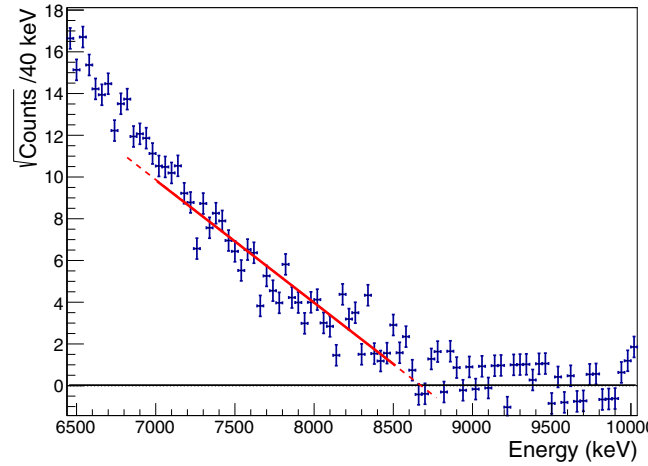

FIG. 7. End point of the EC-decay spectrum of $^{152}\mathrm{Tm}_{9^+}$ measured with the TAS. The spectrum represents the square root of the number of counts as a function of the energy as done in Ref. [41]. The solid line is a linear fit within the range 7000 to 8500 keV. The dashed line is just to guide the eye to the crossing point with the 0.

We should mention here that the observation of the tail of the GT resonance has considerable importance in the discussion of the "quenching" of the GT strength. One of the arguments in this discussion is that the strength is not quenched but hidden in the long background underneath the resonance and extending up to high energies as one sees in charge-exchange reaction experiments [42] and references therein. The present case and the other cases discussed here show for the first time the tail of the resonance measured in β decay and therefore free of background ambiguities, in particular the isovector spin monopole (IVSM) contribution. Reaction experiments carried out with hadronic probes always contain some IVSM strength mixed with the GT excitations spreading along the tail above the GT resonance, this one being of the major uncertainties in identifying the B(GT) strength in the continuum (see Ref. [42] and references therein).

IV. SYSTEMATICS OF THE GT RESONANCE IN THE REGION

In this work (together with Ref. [14]) we have studied the β decay of the odd-Z, $N = 83$ ^{152}Tm, ^{150}Ho, and ^{148}Tb nuclei. In this way we have covered the systematics of the $\pi h_{11/2} \rightarrow \nu h_{9/2}$ decay in the region as we fill the $h_{11/2}$ orbital with approximately 0 to 5 protons (which from now on we

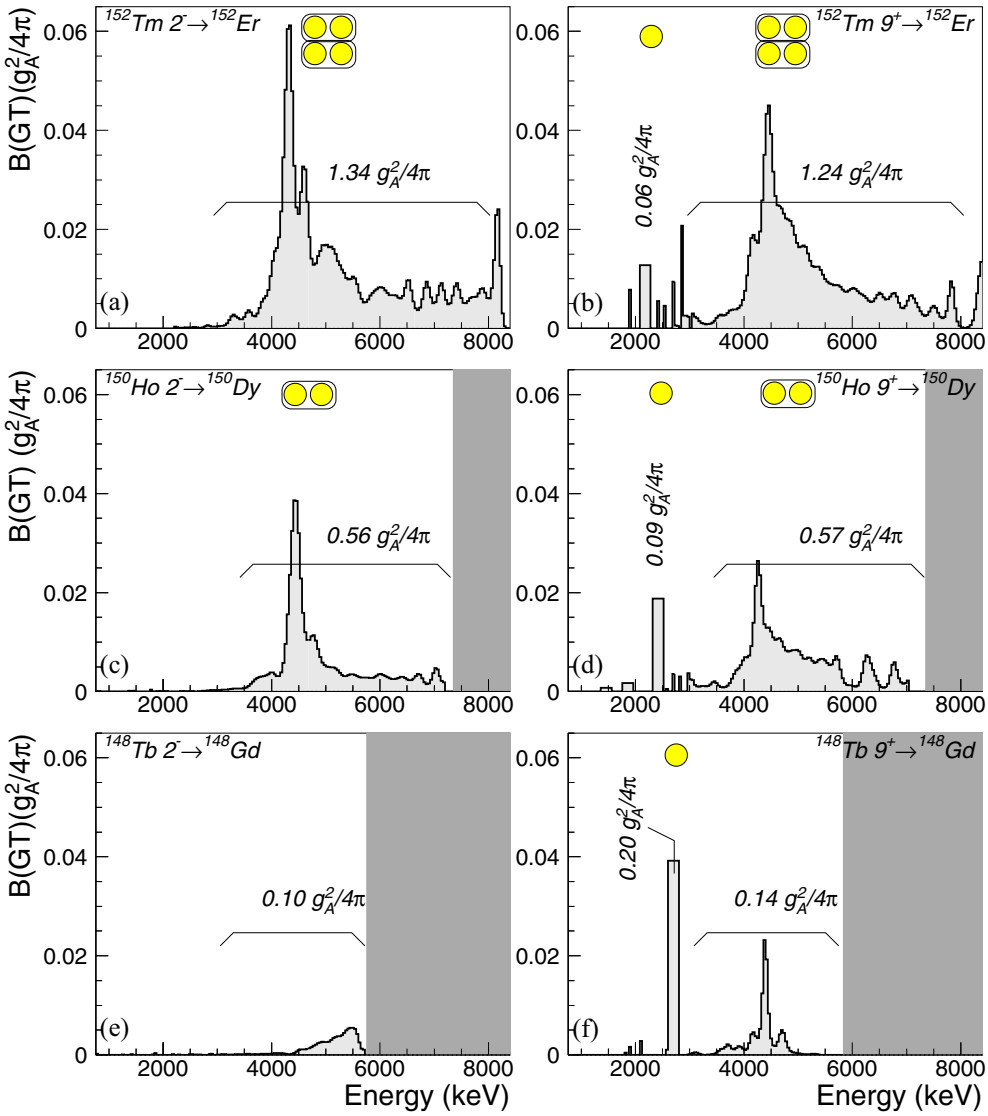

FIG. 8. GT strength distribution in the β decay of the odd-Z, $N = 83$ nuclei above ^{146}Gd pertinent to the present discussion. The left column (a),(c),(e) corresponds to the 2^- isomer and the right column (b),(d),(f) to the 9^+ isomer. From the bottom to the top we have first the decay of ^{148}Tb, which covers the cases with 0 (e) and 1 (f) proton in the $h_{11/2}$, then the decay of ^{150}Ho, corresponding to the cases with 2 (c) and 3 (d) protons and at the top ^{152}Tm, covering the cases with 4 (a) and 5 (b) protons in the $h_{11/2}$. The shading at the right-hand side of each graph represents the region beyond the $Q_{\rm EC}$ value which is inaccessible in the decay. The circles at the top of each graph represent schematically the number of protons above the $Z = 64$ gap involved in the decay in an extreme single-particle approximation.

will call 0, 1, 2, . . . protons in the $h_{11/2}$). In Fig. 8 we present the results of our measurements for the B(GT) distribution using the TAS technique in the six cases. The left column corresponds to the 2^- isomer and the right column to the 9^+ isomer. From the bottom to the top we have first the decay of ^{148}Tb, which covers the cases with 0 and 1 proton in the $h_{11/2}$, then the decay of ^{150}Ho, corresponding to the cases with 2 and 3 protons and studied in Refs. [14,15], and at the top ^{152}Tm, covering the cases with 4 and 5 protons in the $h_{11/2}$. The shading at the right-hand side of each graph represents the region beyond the $Q_{\rm EC}$ value which is inaccessible in the decay. The circles at the top of each graph represent schematically the number of protons above the $Z = 64$ gap involved in the decay. They have been separated into two different categories: the odd valence proton in the $h_{11/2}$ orbital and the 0^+ proton pairs shared among the three orbitals $s_{1/2}$, $d_{3/2}$, and $h_{11/2}$. As mentioned in the Introduction, from the shell-model point of view, any GT transition can only originate from the protons occupying the $h_{11/2}$ orbital; thus, for simplicity, we refer to these decays as the decay of the odd proton or the decay of the proton pairs. When the decay involves the odd proton, it populates mainly one single 8^+ state of two-particle (2p) character; however, the decay of a proton pair populates states of four-particle (4p) character in the broad distribution at higher energy. The amount of B(GT) to the 2p state or to the 4p states is given in Fig. 8 in units of $g_A^2/4\pi$. The first common feature in all cases apart from ^{148}Tb 2^- is the relatively narrow resonance with its maximum at $\approx$4.5 MeV in the daughter nucleus. The position of the resonance is in agreement with our first-order estimate of 4–5 MeV; see

Sec. I of this article. The resonance in ^{148}Tb requires the promotion of proton pairs from below to above the energy gap at $Z = 64$ in the core and its position is discussed later. The width of the resonance has two different components (besides the experimental resolution): spreading width and escape width. The former is attributable to configuration mixing and the latter is given by the half-lives of the states populated which can be very short if they are particle unbound. In our case, the GT state decays mainly by γ emission instead of particle emission; therefore, the corresponding escape width is negligible for the present discussion. In fact, the β-delayed α emission has been measured in the case of ^{150}Ho 2^- and ^{152}Tm 2^- [43], and it was found that it makes a small contribution to the B(GT) compared with the γ emission and affects the half-life of the levels very little. The fact that the GT state is mixed with many other states of particle character (1p, 2p, 3p, ...) or particle-hole character (1p1h, 2p2h, 3p3h, ...) is what we regard as configuration mixing and we conclude that this is the main contribution to the observed width. In Fig. 8 we see a full width at half maximum (FWHM) of the order of 400–500 keV for the decay of ^{152}Tm 2^- and 250 keV for the decay of ^{150}Ho 2^-. The corresponding high-spin cases seem to have part of the B(GT) resonance shifted towards higher energies increasing the area in the tail of the resonance beyond the main peak. In the case of ^{148}Tb we observe a bigger spread of the resonance in the decay of the 2^- isomer and an extremely narrow resonance in the high-spin case with a FWHM of 120–150 keV. We conclude that the spreading width, owing to configuration mixing, grows rapidly with the number of particles in the final nucleus. This is because, as the number of valence particles increases, there are more possible combinations of particles to build up complex configurations with the proper J^π which can mix; therefore, some B(GT) goes to these states. This mixing is also responsible for the long tail beyond the peak which is cut by the $Q_{\rm EC}$ window in most of the cases. According to Ref. [44], this tail can reach ≈200 MeV, carrying up to 50% of the total GT strength. This is in accord with our observations even in the restricted energy range accessible in our measurements.

Let us now take a closer look at the B(GT) values shown in Fig. 8 and summarized in Table I.

The second row of the table shows the occupation of the $h_{11/2}$ orbital expected in an extreme single-particle picture, and the third row shows the experimental B(GT) values. As mentioned above, the total B(GT) going to the lower state and to the resonance must be related to the occupation of protons in the $h_{11/2}$ orbital, but clearly the extreme single-particle approximation is too simplistic. To obtain a more realistic estimate of these quantities we have performed a shell-model calculation using the OXBASH code [45]. In this calculation we have taken ^{146}Gd as a core for the ^{150}Ho and ^{152}Tm cases and we have included the $s_{1/2}$, $h_{11/2}$, and $d_{3/2}$ orbitals above the core. We return to ^{148}Tb later. We have used empirical single-particle energies and two-body interaction matrix that were estimated from experimental data (see Ref. [9] for a description of the method originally developed by Blomqvist [46]). All the nondiagonal matrix elements have been neglected except for those related to the pairing correlations, i.e., the three 0^+ two-body interactions $\langle \pi s^2_{1/2}|V|\pi d^2_{3/2}\rangle_{0^+}$, $\langle \pi s^2_{1/2}|V|\pi h^2_{11/2}\rangle_{0^+}$, and $\langle \pi d^2_{3/2}|V|\pi h^2_{11/2}\rangle_{0^+}$. These three, and the three diagonal terms $\langle \pi s^2_{1/2}|V|\pi s^2_{1/2}\rangle_{0^+}$, $\langle \pi d^2_{3/2}|V|\pi d^2_{3/2}\rangle_{0^+}$, and $\langle \pi h^2_{11/2}|V|\pi h^2_{11/2}\rangle_{0^+}$ have been adjusted to reproduce the 0^+, $2^+, \ldots, 10^+$ yeast levels in ^{148}Dy[1]. Looking at the wave functions obtained in this calculation we can estimate the number of protons in the $h_{11/2}$ orbital for the isomers in both ^{150}Ho and ^{152}Tm and these numbers are given in the fourth row of the table.

To estimate the proton occupation probability for the case of ^{148}Tb we could perform shell-model calculations similar to those for the other cases but this would require the inclusion of the $d_{5/2}$ and $g_{7/2}$ orbitals, thus making the calculations more complicated. A possible alternative is to turn the problem around and try to deduce the scattering of pairs across the $Z = 64$ gap from a comparison of the decays of ^{148}Dy and ^{148}Tb$_{2^-}$. Assuming that the B(GT) is directly proportional to the number of pairs in the $h_{11/2}$ orbital, we can write

$$\frac{B(\mathrm{GT})_{^{148}\mathrm{Dy}}}{B(\mathrm{GT})_{^{148}\mathrm{Tb}\ 2^-}} = \frac{0.67 + p}{p}, \tag{3}$$

where in the second term we have "0.67", the number of proton pairs in the $h_{11/2}$ orbital in the ground state of ^{148}Dy from our shell-model calculation, which does not include the scattering of pairs across the $Z = 64$ gap, and "p", which is the number

[1]These calculations predict two 0^+ states at 2.85- and 3.26-MeV excitation energy so far not identified.

TABLE I. B(GT) values measured and calculated for the six isomeric decays studied in this work. The first row lists the six cases studied. The second row shows the occupation of the $h_{11/2}$ orbital expected in an extreme single-particle picture. The third row shows the experimental B(GT) values. For the 9^+ isomers, the total B(GT), as well as the amount of B(GT) going to the lower state and to the resonance, are specified. The fourth row shows the proton occupation of the $h_{11/2}$ orbital estimated empirically for ^{148}Tb and from a shell-model calculation for the others (see text). The last row shows the experimental B(GT) value normalized to the ^{148}Tb$_{9^+}$ case (see text).

	^{148}Tb 2^-	^{148}Tb 9^+	^{150}Ho 2^-	^{150}Ho 9^+	^{152}Tm 2^-	^{152}Tm 9^+
$N(h_{11/2})_{\rm s.p.}$	0	1	2	3	4	5
B(GT) $(g_V^2/4\pi)$	0.10(1)	0.34(4) $\{^{0.20(2)}_{0.14(2)}$	0.56(4)	0.66(7) $\{^{0.09(1)}_{0.57(7)}$	1.3(2)	1.26(3) $\{^{0.06(1)}_{1.2(3)}$
$N(h_{11/2})_{\rm calc}$	0.3	1.3	1.5	2.3	3.0	3.6
$B(\mathrm{GT})_{\rm norm}$(a.u.)	0.29(3)	1.0(1) $\{^{0.59(6)}_{0.41(6)}$	1.7(1)	1.9(2) $\{^{0.26(3)}_{1.7(2)}$	3.8(6)	3.7(8) $\{^{0.17(3)}_{3.5(9)}$

of extra *scattered pairs* that we want to calculate. We are neglecting the small blocking effect of the proton in the $d_{3/2}$ in ^{148}Tb$_{2^-}$, which allows us to assume that the number of scattered proton pairs p is the same for ^{148}Dy and ^{148}Tb$_{2^-}$. We can solve Eq. (3) for p:

$$p = 0.67 \times \left[\frac{B(\mathrm{GT})_{^{148}\mathrm{Dy}}}{B(\mathrm{GT})_{^{148}\mathrm{Tb}\ 2^-}} - 1 \right]^{-1}. \quad (4)$$

If we use our results for the total B(GT) measured for the decay of ^{148}Tb$_{2^-}$ and the B(GT) in the decay of ^{148}Dy taken from Ref. [47], we find that the number of proton pairs scattered upwards from the ^{146}Gd core is

$$p = 0.15(3).$$

This number multiplied by two gives a good estimate for the number of protons in the $h_{11/2}$ orbital in the ^{148}Tb$_{2^-}$ case. For the ^{148}Tb$_{9^+}$ isomer we have to add one extra proton; consequently, the estimated number of protons in this case is $1 + 0.30$. These two numbers complete the fourth row of the table.

Incidentally, we note that the obtained $p = 0.15(3)$ can be compared with the same number for ^{144}Sm, which is 0.80(15) according to Ref. [48]. This comparison indicates that, owing to the increase in the gap at $Z = 64$ in ^{146}Gd with respect to ^{144}Sm, the scattering of proton pairs across the gap is much smaller (a factor of 5) in the nuclei above the ^{146}Gd core than in the nuclei below the core. This reinforces the quasi-doubly magic character of ^{146}Gd.

To compare the estimated number of protons in the $h_{11/2}$ orbital with the measured B(GT), we have renormalized the B(GT) values arbitrarily to one unit for the ^{148}Tb$_{9^+}$ case. These values are given in the fifth row of Table I. Comparing the fourth and the fifth rows in the table, we conclude that there is a good agreement between the calculated occupational number for the $h_{11/2}$ orbital and the measured B(GT) values.

Let us now inspect how the B(GT) is distributed in the case of the high-spin isomer between the low-lying 8^+ state, identified as $2p$ state, and the broad resonance at 4.5 MeV, identified as consisting of $4p$ states. Again in the extreme single-particle picture one would expect the B(GT) to the low 8^+ state to remain constant for the three cases and the ratio between the B(GT) to the lower state and to the resonance to be 1/0 in Tb, 1/2 in Ho, and 1/4 in Tm. How different these expectations are from the reality is best discussed looking at the fifth row of the table where the values for the lower state and the resonance are given separately. We observe that the strength to the lower 8^+ state does not stay constant; on the contrary, it decreases as we increase the number of protons in the $h_{11/2}$ orbital ($0.59 \rightarrow 0.26 \rightarrow 0.17$). Moreover, the missing strength from the lower 8^+ is shifted to the resonance region.

Actually, this effect has been observed for some years in charge-exchange reaction experiments, but not as clearly as in the present case and never in β-decay studies. It is normally attributed to a residual repulsive interaction which mixes the pure states, moves them apart, and redistributes the strength. One example is presented in Ref. [49], in which the authors show some experimental results from the ^{48}Ca(^{3}He,t)^{48}Sc reaction and explain the distribution of the GT strength in terms of shell-model calculations. To a first approximation the strength is shared between the two pure states, namely $\pi f_{7/2} \nu f_{7/2}^{-1}$ and $\pi f_{5/2} \nu f_{7/2}^{-1}$. As soon as one considers the mixing between both states using a particular particle-hole interaction extracted from Ref. [50] both states are pushed up, and the GT strength originally placed in the low-lying state is reduced by a factor of three and moved to the upper state.

How this effect depends on the number of valence particles is discussed in Ref. [51], where the authors find, for the ^{42}Ca(p,n)^{42}Sc reaction, that the strength is concentrated in the lower state and only a small fraction of it moves towards higher energy. However, as one adds neutrons to the system [e.g., the ^{48}Ca(^{3}He,t)^{48}Sc reaction mentioned above] the GT strength moves from the lower to the higher states. The authors of Ref. [51] attribute this effect to the fact that the particle-particle matrix elements relevant for ^{42}Sc are attractive, whereas the particle-hole matrix elements relevant for ^{48}Sc are repulsive. A similar discussion can be found in the more recent work of Fujita *et al.* [52]. In the present case we have observed in our data that the GT strength moves up gradually from the lower state (the 8^+ $2p$ state) to the higher states (the $4p$ ones at $\approx$4.5 MeV) as the number of protons is increased, which is exactly the same effect as found in Ref. [51] with the increase in the number of neutrons. We note, however, that in our case we are dealing with states of particle character and not with holes so we conclude that the residual interaction increases its repulsive character with the number of protons.

So far the discussion has been focused on the relative B(GT) values more than on the absolute values. At this point one can compare the results obtained in this work for the total B(GT) with theoretical estimates of Towner in Ref. [53]. It is worth noting here that the calculations of Ref. [53] refer to $N = 82$ and we compare them with our results for $N = 83$ nuclei. In this we assume that the valence neutron in the parent state is in the $f_{7/2}$ orbital, which does not take part in the decay and consequently does not affect the B(GT). The comparison of the expected values for the total B(GT) using Ref. [53] and our measurements is shown in Fig. 9. On the x axis of the graph we show the number of protons in the $h_{11/2}$ proton orbital in the extreme single-particle picture and on the y axis the total B(GT). The black vertical bars represent the calculation [53]. The lengths of the bars represent the range of possible B(GT) values depending on the choice of the effective interaction in the evaluation of the core polarization in Ref. [53]. The gray squares with error bars are the values measured for the total B(GT) using the total absorption technique. The points corresponding to the decay of the two isomers in ^{150}Ho have been taken from Ref. [14], and the remainder are the results of this work. Although the experimental points follow a similar trend to the theory, they are systematically lower. There can be at least two reasons for this. From the theoretical point of view the calculation is performed using a very limited configuration space in the sense that the author only takes into account the $h_{11/2}$ orbital for the protons and the $h_{9/2}$ for the neutrons. This extreme picture is corrected using pairing correlation corrections, core polarization, and higher order effects, but not by the possible mixing of the originally assumed states of $2p$ character (in our case of $2p$ or $4p$ character) with many other

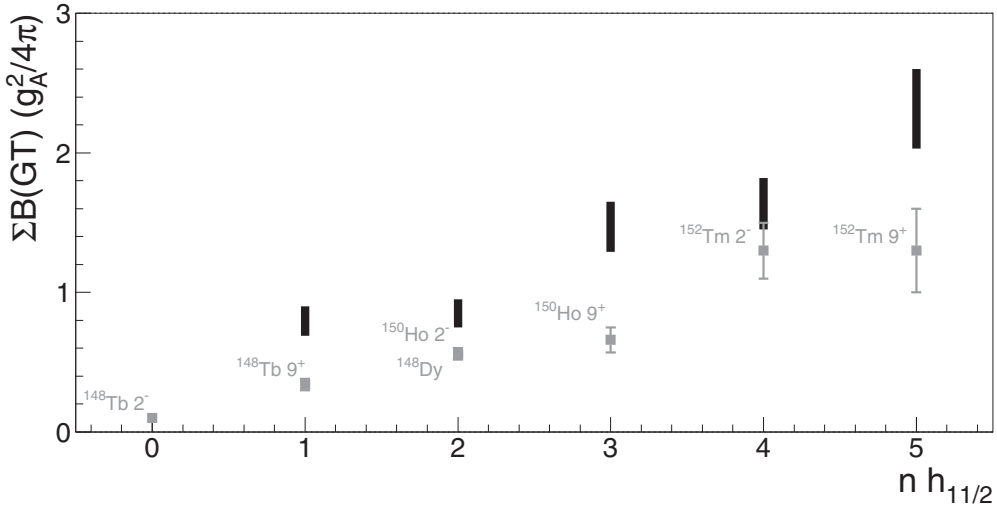

FIG. 9. Evolution of the total B(GT) as a function of the occupancy number of the proton orbital $h_{11/2}$. The results from this work (gray squares) are compared with the theoretical estimates of Ref. [53] (black bars).

more complex configurations lying at higher excitation energy. However, from the experimental point of view we assume that we measure all the B(GT) which lies inside the Q_{EC} window. If the strength is shifted to higher energies and lies beyond the Q_{EC}, we will miss this fraction. This is also what we expect observing the tail of the resonance extending up to the Q_{EC} value and agrees with the postulate of Bertsch and Hamamoto [44], giving the same argument but from a theoretical point of view. In summary, we conclude that the discrepancy observed in Fig. 9 between calculation and experiment is attributable to the strength that is shifted towards higher energies by configuration mixing, thus producing the tail clearly observed in the experiments that is cut off by the Q_{EC}. This idea is reinforced by the fact that the discrepancy is more marked for the high-spin isomer decay. As discussed above, it is for these cases that the tail of the resonance is more prominent.

V. DISCUSSION OF THE B(GT) DISTRIBUTION AND COMPARISON WITH SHELL-MODEL CALCULATIONS

In the previous section we discussed the B(GT) strength extracted from our data in detail. So far, however, we have not discussed the position of the resonance in accurate terms; we have only given an indication of the expected excitation energy. In this section we estimate the excitation energy of the states primarily populated in the β decay. This is done in the framework of shell-model calculations described before. However, for the decay of ^{148}Tb we cannot use the same core as this would require the inclusion of the $d_{5/2}$ and $g_{7/2}$ orbitals making the calculations considerably more complex as stated before. To avoid this complexity we have used a different core: ^{144}Sm. Using the same approach developed in Ref. [46], we constructed a two-body interaction matrix for the calculation of the states in ^{148}Gd that are populated in the β decay of ^{148}Tb. These states are, in the low-spin case, $4p$ states with the configuration $[\pi d_{3/2}\pi h_{11/2}\nu f_{7/2}\nu h_{9/2}]_{1^-,2^-,3^-}$ [see Fig. 1(a)]. In the high-spin case the configurations will be the 4p states populated in the breakup of a proton pair, $[\pi h_{11/2}\pi h_{11/2}\nu f_{7/2}\nu h_{9/2}]_{8^+,9^+,10^+}$, and the $2p$ state populated in the decay of the odd proton, $[\pi h^2_{11/2}]_{0^+}[\nu f_{7/2}\nu h_{9/2}]_{8^+}$ [see Fig. 1(b)]. As the nucleus that acts as a core for this shell-model calculation is ^{144}Sm, the values for the single-particle excitations and for the residual two-body interaction are taken from experimental data relative to this core. We neglected all the nondiagonal terms of the interaction matrix except the ones related to the pairing correlations of the protons, which are $\langle \pi s^2_{1/2}|V|\pi d^2_{3/2}\rangle_{0^+}$, $\langle \pi s^2_{1/2}|V|\pi h^2_{11/2}\rangle_{0^+}$, and $\langle \pi d^2_{3/2}|V|\pi h^2_{11/2}\rangle_{0^+}$. These three and the three diagonal terms $\langle \pi s^2_{1/2}|V|\pi s^2_{1/2}\rangle_{0^+}$, $\langle \pi d^2_{3/2}|V|\pi d^2_{3/2}\rangle_{0^+}$, and $\langle \pi h^2_{11/2}|V|\pi h^2_{11/2}\rangle_{0^+}$ have been adjusted to reproduce the ^{146}Gd level scheme.

Once we know the single-particle energies and the two-body interaction matrix is constructed, one can run the OXBASH code to calculate the wave functions and energies of the states in the daughter nucleus. For the decay of ^{148}Tb 2^- we only needed to calculate the 1^-, 2^-, and 3^- states in ^{148}Gd (because other states are not directly populated in allowed GT transitions). In the next step one calculates the wave function of the parent state, and finally the matrix elements of the $\sigma\tau$ operator between the parent and daughter states. The squares of these matrix elements are proportional to the reduced transition probabilities: B(GT).

The results of our shell-model calculation for the low-spin isomeric decays are presented in Fig. 10. The direct results from the OXBASH calculation have been folded with a Gaussian distribution (FWHM $\approx$ 165 keV) to account for the width of the experimental distribution, which is attributable to mixing of configurations not included in the calculation. The normalization of the total area of the shell-model results is completely arbitrary; it has been chosen to give the same height for the measured and the calculated resonance. We can see that even with a very restricted phase-space calculation we can reproduce the position of the measured GT resonance within less than half MeV in the worst case (^{152}Tm$_{2^-}$ in the top panel).

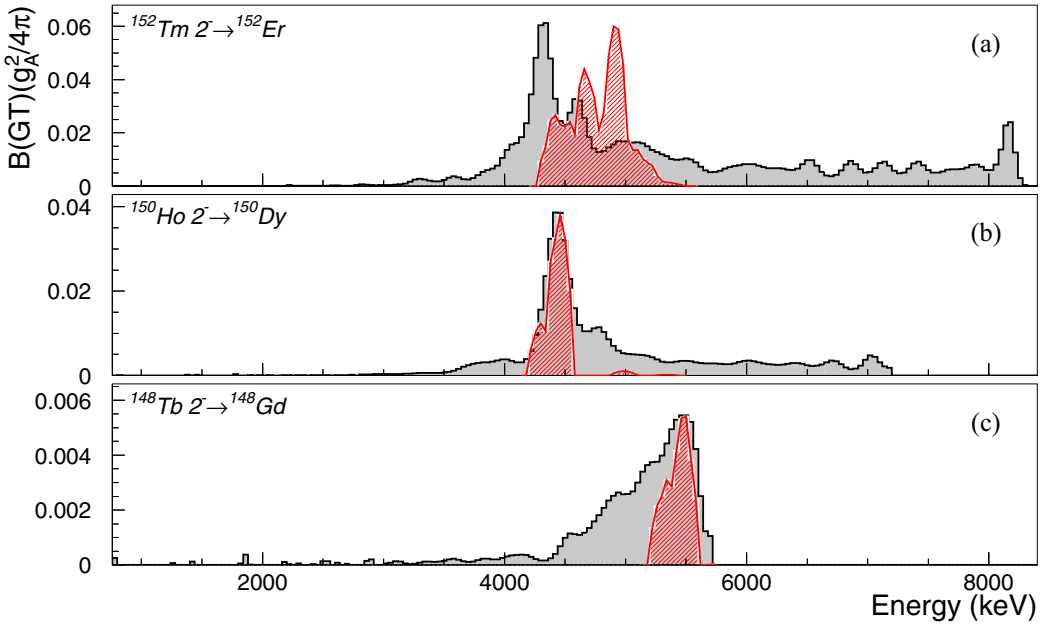

FIG. 10. GT strength distribution for the low-spin isomer of the odd-Z, $N = 83$ nuclei above ^{146}Gd. The results from the TAS measurement (black/gray) are compared with a shell-model calculation (red).

To calculate the high-spin cases we proceeded in the same way: We took the two-body interaction matrix elements from Ref. [9] and, using ^{146}Gd as a core, we calculated the 8^+, 9^+, and 10^+ states in the daughter nuclei ^{152}Er and ^{150}Dy. Afterwards we calculated the wave functions of ^{152}Tm$_{9^+}$ and ^{150}Ho$_{9^+}$, and then we ran the code to obtain the GT amplitudes. After that, we used the two-body interaction matrix that we used for the ^{148}Tb$_{2^-}$ case and we took ^{144}Sm as the core to perform a similar calculation for the decay of ^{148}Tb$_{9^+}$. The results of these calculations for the high-spin isomeric decays are presented in Fig. 11. One can observe that the calculated strength actually moves from the lower state to the upper ones as we add protons to the $h_{11/2}$ orbital. This is the effect we discussed in the previous section in reference to our work and to the results from Ref. [51]. Besides that, the agreement between theory and experiment is not as good as in the low-spin cases. For the case of ^{152}Tm$_{9^+}$ and ^{150}Ho$_{9^+}$ decays, it is still acceptable in terms of the position of the centroid of the resonance; however, the calculated distribution presents a splitting that we do not observe experimentally, especially in the case of ^{150}Ho$_{9^+}$ decay.

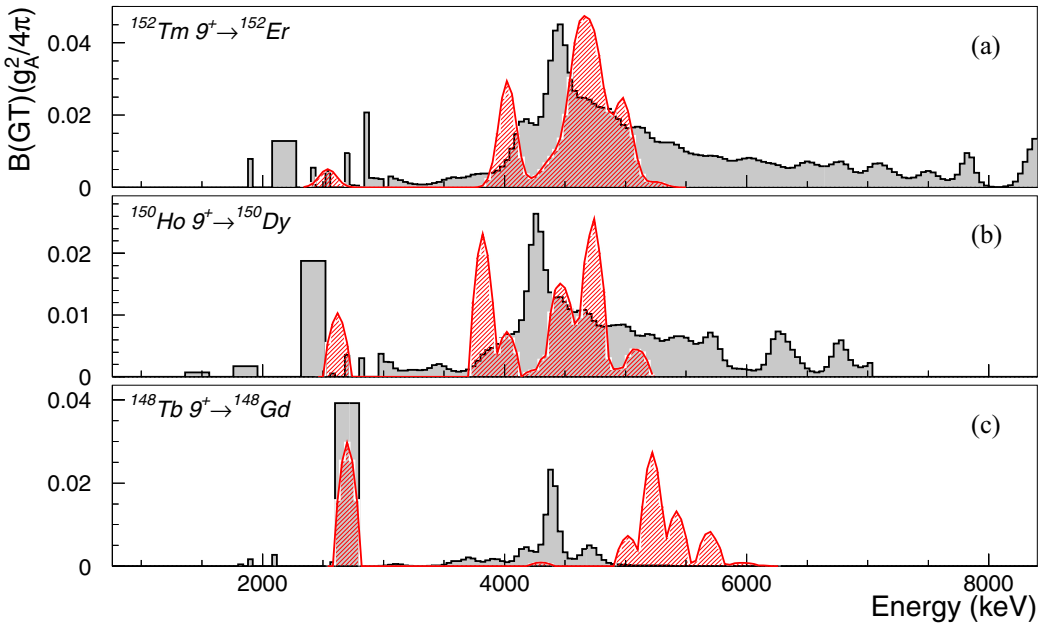

FIG. 11. Same as Fig. 10 but for the high-spin isomers.

The case that presents the largest difference between theory and experiment is the decay of ^{148}Tb$_{9^+}$, in which the centroid of the theoretical distribution is shifted by almost 1 MeV with respect to the measured one. Actually, in different sections we have made clear that the B(GT) distribution in the decay of ^{148}Tb should be shifted with respect to the same distribution in the other decays of the odd-Z, $N = 83$ nuclei above ^{146}Gd because one proton pair must be promoted from the core in the case of ^{148}Tb and this requires some extra energy. In fact, the shell-model calculation reproduces very well the position of the resonance in the decay of the low-spin isomer of ^{148}Tb (see Fig. 10). However, the decay of the high-spin isomer does not present the same distribution shifted with respect to the other decays and it is difficult to imagine why in this case the breakup of a proton pair promoted from the core should be different from the same breakup of a proton pair in the low-spin case. One possible explanation lies in the reduced configuration space we are using, in particular on the absence of the $d_{5/2}$ and $g_{7/2}$ orbitals below the $Z = 64$ gap. This blocks the possibility of building two-hole states that are part of the $4p$ states populated in the resonance and above.

VI. SUMMARY AND CONCLUSIONS

We have measured the distributions of GT strength to states populated in the β decay of the low- and high-spin isomers in ^{148}Tb, ^{152}Er, and ^{152}Tm using the TAS technique at the GSI On-line Mass-Separator. The measurements also provided the first experimental value for the excitation energy of the ^{152}Tm 9^+ isomer.

These decays can be viewed as being attributable to the allowed decay of protons occupying the $h_{11/2}$ orbital into the empty neutron $h_{9/2}$ orbital where we vary the number of protons involved from 0 to 5. In the data we could clearly identify the decay of the unpaired proton to a single state in the daughter nucleus at ∼2 MeV and the decay of the paired protons to a GT resonance at ∼4.5 MeV.

The strength, as well as the position of the resonance, is well understood based on simple considerations and the help of shell-model calculations (except for the case of ^{148}Tb 9^+ decay).

To our knowledge these are the cases where the GT resonance has been most clearly seen in β decay. A similar resonance is observed in charge exchange reactions at higher excitation energy where the GT resonance has been studied intensively.

Another important result is that in the four cases where the resonance is strong, the tail is seen extending up to the limit imposed by the Q_{EC} value. These are the first cases where the tail of the resonance has been clearly seen in β decay. This observation is of great importance because it has been discussed in the framework of the quenching of the GT strength that part of the missing strength could be hidden in the tail of the resonance. In charge exchange reactions, however, where most of these studies have been carried out, the background at high excitation energy is difficult to interpret despite careful analyzes that have been performed, e.g., in Ref. [42]. In our case, the tail of the resonance is observed without background ambiguities.

The total B(GT) measured in our experiments has been compared with the calculations of Towner [53]. He calculated how the B(GT) should change as a function of the occupation of the $\pi h_{11/2}$ orbital. The general behavior calculated by Towner is well reproduced by the measurements, although strength is missing systematically when we compare experiment with theory. This can be related to the fact that we observed the tail of the resonance up to the Q_{EC} value and there is probably still strength beyond this limit that we cannot reach. This interpretation is corroborated by the fact that the missing strength is more pronounced in the decay of the 9^- isomers where the tail is higher.

ACKNOWLEDGMENTS

The authors would like to thank the GSI accelerator crew and the MSEP group for their support. This work has been partially supported by the Spanish Ministry (Grants No. FPA2005-03993, No. FPA200806419-C02-01, No. FPA2011-24553, No. FPA2012-32443, No. FPA2014-57196-C5, and No. FPA2014-52823-C2-1-P) and the Generalitat Valenciana (PROMETEOII/2014/019).

[1] Y. Fujita *et al.*, Prog. Part. Nucl. Phys. **66**, 549 (2011).
[2] E. Poirier *et al.*, Phys. Rev. C **69**, 034307 (2004).
[3] E. Nácher, A. Algora, B. Rubio, J. L. Tain, D. Cano-Ott, S. Courtin, P. Dessagne, F. Maréchal, C. Miehé, E. Poirier, M. J. G. Borge, D. Escrig, A. Jungclaus, P. Sarriguren, O. Tengblad, W. Gelletly, L. M. Fraile, and G. Le Scornet, Phys. Rev. Lett. **92**, 232501 (2004).
[4] A. Pérez-Cerdán *et al.*, Phys. Rev. C **84**, 054311 (2011).
[5] C. B. Hinke *et al.*, Nature (London) **486**, 341 (2012).
[6] Z. Hu *et al.*, Phys. Rev. C **60**, 024315 (1999).
[7] Z. Hu *et al.*, Phys. Rev. C **62**, 064315 (2000).
[8] M. Gierlik *et al.*, Nucl. Phys. A **724**, 313 (2003).
[9] A. Algora *et al.*, Phys. Rev. C **68**, 034301 (2003).
[10] P. Kleinheinz *et al.*, Z. Phys. A **284**, 351 (1978).
[11] P. Kleinheinz *et al.*, Z. Phys. A **286**, 27 (1978).
[12] L. Caballero, B. Rubio, P. Kleinheinz, S. W. Yates, A. Algora, A. Dewald, A. Fitzler, A. Gadea, J. Jolie, R. Julin, A. Linnemann, S. Lunardi, R. Menegazzo, O. Möller, E. Nácher, M. Piiparinen, and J. Blomqvist, Phys. Rev. C **81**, 031301(R) (2010).
[13] P. Kleinheinz *et al.*, Z. Phys. A **290**, 279 (1979).
[14] D. Cano Ott, Ph.D. thesis, Universidad de Valencia, 2000.
[15] J. L. Tain, D. Cano-Ott, and B. Rubio, *Experimental Nuclear Physics in Europe 1999*, edited by B. Rubio *et al.*, AIP Conf. Proc. No. 495 (AIP, Melville, New York, 1999), p. 97.
[16] J. C. Hardy *et al.*, Phys. Lett. B **71**, 307 (1977).
[17] C. L. Duke *et al.*, Nucl. Phys. A **151**, 609 (1970).
[18] B. Rubio *et al.*, J. Phys G **31**, S1477 (2005).
[19] M. Karny *et al.*, Nucl. Inst. Methods B **126**, 411 (1997).

[20] K. H. Burkard *et al.*, Nucl. Instrum. Methods **139**, 275 (1976).
[21] P. Kleinheinz, R. Barden, R. Kirchner, O. Klepper, A. Plochocki, E. Roeckl, B. Rubio, and D. Schardt, *KFA Jülich Annual Report 1988, JUL-Spez-499* (1989), p. 34.
[22] R. Kirchner and E. Roeckl, Nucl. Instrum. Methods **133**, 187 (1976).
[23] N. Q. B. Gove and M. J. Martin, Nucl. Data Tables A **10**, 205 (1971).
[24] D. Cano *et al.*, Nucl. Instrum. Methods A **430**, 333 (1999).
[25] A. P. Dempster, N. M. Laird, and D. B. Rubin, J. R. Stat. Soc. B **39**, 1 (1977).
[26] J. L. Tain and D. Cano-Ott, Nucl. Instrum. Methods A **571**, 719 (2007).
[27] J. L. Tain and D. Cano-Ott, Nucl. Instrum. Methods A **571**, 728 (2007).
[28] S. Agostinelli *et al.*, Nucl. Instrum. Methods A **506**, 250 (2003), http://wwwasd.web.cern.ch/wwwasd/geant4/geant4.html
[29] K. S. Toth, D. C. Sousa, J. M. Nitschke, and P. A. Wilmarth, Phys. Rev. C **35**, 310 (1987).
[30] A. Algora *et al.*, in *"ENAM2001" Conference Proceedings*, edited by J. Äystö *et al.* (Springer, Berlin, 2001), p. 345.
[31] A. Algora (private communication).
[32] J. Kopecky and M. Uhl, Phys. Rev. C **41**, 1941 (1990).
[33] J. C. Hardy *et al.*, Phys. Lett. B **109**, 242 (1982).
[34] J. Speth *et al.*, Rep. Prog. Phys. **44**, 719 (1981).
[35] W. V. Prestwich *et al.*, Z. Phys. A **315**, 103 (1984).
[36] J. C. Hardy and I. S. Towner, Phys. Rev. C **79**, 055502 (2009).
[37] J. C. Hardy and I. S. Towner, Nucl. Phys. News **16**, 11 (2006).
[38] E. Nolte *et al.*, Z. Phys. A **309**, 33 (1982).
[39] M. Wang *et al.*, Chin. Phys. C **36**, 1603 (2012).
[40] G. Audi *et al.*, Chin. Phys. C **36**, 1157 (2012).
[41] G. D. Alkhazov *et al.*, Z. Phys. A **344**, 425 (1993).
[42] M. Ichimura, H. Sakai and T. Wakasal, Prog. Part. Nucl. Phys. **56**, 451 (2006).
[43] E. Nácher *et al.*, *The 4th International Conference on Proton Emitting Nuclei and Related Topics*, edited by B. Blank, AIP Conf. Proc. No. 1409 (AIP, Melville, New York, 2011), p. 181.
[44] G. F. Bertsch and I. Hamamoto, Phys. Rev. C **26**, 1323 (1982).
[45] B. A. Brown *et al.*, MSU-NSCL Report No. 524 (1988).
[46] J. Blomqvist *et al.*, Z. Phys. A **312**, 27 (1983).
[47] A. Algora, E. Nácher, B. Rubio, D. Cano-Ott, J. L. Tain, A. Gadea, J. Agramunt, M. Karny, Z. Janas, K. Rykaczewski, R. Collatz, M. Hellström, Z. Hu, R. Kirchner, E. Roeckl, M. Shibata, L. Batist, F. Moroz, and V. Wittmann, Phys. Rev. C **70**, 064301 (2004).
[48] B. H. Wildenthal *et al.*, Phys. Rev. C **3**, 1199 (1971).
[49] C. Gaarde *et al.*, Nucl. Phys. A **334**, 248 (1980).
[50] C. Gaarde *et al.*, Nucl. Phys. A **222**, 579 (1974).
[51] H. Toki and G.F. Bertsch, Phys. Rev. C **26**, 2330 (1982).
[52] Y. Fujita *et al.*, Phys. Rev. Lett. **112**, 112502 (2014).
[53] I. S. Towner, Nucl. Phys. A **444**, 402 (1985).